High Power Laser Science and Engineering, (2025), Vol. 13, e58, 12 pages.
doi:10.1017/hpl.2025.10053

HIGH POWER LASER SCIENCE AND ENGINEERING

RESEARCH ARTICLE

A 0.82 μm, 105 W diode-pumped thulium-doped all-silica-fiber laser

Changshun Hou, Ziwei Zhai, Nilotpal Choudhury, Tom Harris, Qiubai Yang, Jayanta K. Sahu, and Johan Nilsson

Optoelectronics Research Centre, University of Southampton, Southampton, UK

(Received 29 May 2025; revised 2 July 2025; accepted 7 July 2025)

Abstract

An all-silica-fiber thulium-doped fiber laser emitting at 0.82 μm on the transition from $^3H_4$ to the ground state $^3H_6$ outputs 105 W continuous-wave power and 555 W quasi-continuous-wave instantaneous power with 0.96% duty cycle in 240 μs rectangular pulses. The system comprises a double-clad thulium-doped fiber designed and fabricated in-house, incorporated into an all-fiber cavity and cladding-pumped by diode lasers at 0.79 μm. Co-lasing at 1.9 μm counteracts population trapping in $^3F_4$. The slope efficiency reaches 64% and 77.5% under quasi-continuous-wave and continuous-wave operations, respectively. Under quasi-continuous-wave conditions, the beam quality M^2 becomes 2.2 (beam parameter product: 0.57 mm mrad) and 2.45 (0.64 mm mrad) in orthogonal directions at approximately 250 W of instantaneous output power. In addition, a modified quasi-continuous-wave setup is continuously wavelength-tunable from 812 to 835 nm. We believe this is the first reported demonstration of high-power laser operation of the $^3H_4 \rightarrow {}^3H_6$ transition in a thulium-doped fiber.

Keywords: all-fiberization; diode pumping; high-power fiber laser; thulium-doped silica fiber; wavelength-tunable fiber laser

1. Introduction

An efficient, high-power fiber laser source with high beam quality in the 800 nm spectral region holds strong appeal for applications such as advanced materials processing. While ytterbium-doped fiber lasers (YDFLs) operating at 1.0 or 1.1 μm have become industry standard for laser machining of metals, their performance is significantly constrained when dealing with materials that are highly reflective in that wavelength range, such as aluminum, which plays a crucial role in the aerospace industry and in e-mobility. For example, the need for lightweight aircraft structural parts in aerospace is primarily met by aluminum alloys[1], which are much lighter than steel structures[2]. In addition, aluminum outperforms steel in demanding working conditions, offering superior durability and resilience[3], bringing together properties such as corrosion resistance, strength and rigidity in a single product[4]. As shown in Figure 7 of Ref. [5], aluminum exhibits reflectance exceeding 95% at 1.06 μm, severely compromising energy deposition at that wavelength. In contrast, shorter wavelengths generally exhibit higher absorption in metals[6]. For instance, reducing the laser wavelength from 1.06 μm to 808 nm approximately triples the aluminum absorption, as also illustrated in Figure 7 of Ref. [5]. This enhanced absorption enables more efficient melting at lower laser powers and opens up the way for reduced energy consumption. High beam quality can further improve the processing, offering more uniform heating and melting profiles, minimized defects such as cracks, and greater precision in applications such as surface treatment and welding[7]. In addition to materials processing, a high-power and high beam quality laser source at 0.8 μm is attractive for advancing quantum technologies. For instance, a high-power 813 nm laser can be utilized for optical lattice trapping in strontium, enabling the creation of stable traps for Sr-based optical lattice clocks (OLCs) with minimal perturbation to clock transitions, thus enhancing precision timekeeping. Higher power levels allow for the collection of more ions, further improving the stability and accuracy of OLCs[8]. Furthermore, a high-power 852 nm laser can pump cesium, enabling atomic fountain clocks, interferometry and focused ion beam (FIB) applications, for which high output power is required to increase the atom number and signal-to-noise ratio[9,10].

Correspondence to: C. Hou, Faculty of Engineering and Physical Sciences, University of Southampton, Southampton SO17 1BJ, UK. Email: C.Hou@soton.ac.uk

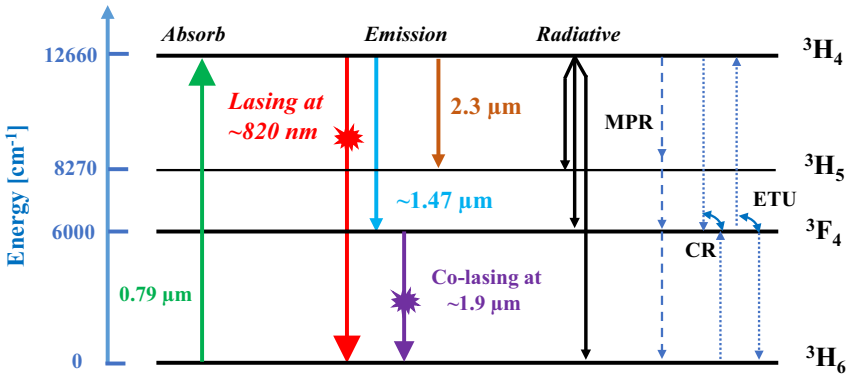

Figure 1. Partial energy-level diagram and transitions of Tm^{3+} ions in silica (MPR, multi-phonon relaxation; CR, cross-relaxation; ETU, energy transfer upconversion).

As another application, 0.8 μm lasers can be used to pump neodymium-doped fiber lasers emitting near 0.9 μm[11,12]. Their three-level nature means they benefit from high pump brightness, making them challenging to power-scale when pumping with diode lasers. By contrast, core-pumping with a high-brightness 0.8 μm laser allows for much shorter gain fibers with higher inversion than with cladding-pumping. This reduces the reabsorption and enables operation on shorter wavelengths of the 0.9 μm transition, potentially even shorter than the absorption peak at approximately 0.89 μm. In addition, single-mode end-pumping of Nd-doped 'bulk' traveling-wave optical amplifiers is attractive since it opens up the way for tight pump-beam confinement and high gain in relatively long gain media, in which a poor beam quality would necessitate much higher pump powers. This has been demonstrated in ytterbium-doped yttrium aluminum garnet (Yb:YAG), where a 17-mm-long crystal reached nearly 40 dB of gain at 1030 nm when pumped with 35 W of power at 920 nm from a single-mode neodymium-doped fiber laser[13].

Despite the attractions of these applications, there is a lack of efficient high-brightness 0.8 μm lasers. The power from commercially available single-mode 0.8 μm diode lasers is limited below the watt level. Although Ti:Al_2O_3 laser sources can emit at those wavelengths, their high cost and complexity and their low overall efficiency limit their practicality. Furthermore, scaling beyond a few tens of watts is challenging.

Cladding-pumped silica fibers doped with Tm^{3+} and operating on the transition $^3H_4 \rightarrow {}^3H_6$ (the ground state) have the potential to fill this gap[14]; see Figure 1 for a partial energy-level diagram and transitions in Tm^{3+}. However, the 1100 cm^{-1} maximum phonon energy of silica glass leads to rapid multi-phonon relaxation (MPR) from $^3H_4$ to $^3H_5$. The resulting short fluorescence lifetime of $^3H_4$ (e.g., 10 μs or a few tens of μs), serving as the upper laser level (ULL), hampers population inversion[15,16]. Consequently, the 0.8 μm transition has received less attention than the well-known 2 μm transition $^3F_4 \rightarrow {}^3H_6$, which benefits from a much longer lifetime of its ULL ($^3F_4$) in Tm-doped silica fibers. We also mention that the $^3H_5$ lifetime is short enough, and the energy gap to $^3F_4$ is large enough, to render its population negligible. Theoretical modeling of a silica-based fiber laser at 810 nm has been detailed by Peterka *et al.*[17] and amplification around this wavelength has been demonstrated in core-pumped silica fiber[18]. Furthermore, we have recently reported amplification on the $^3H_4 \rightarrow {}^3H_5$ transition at 2.3 μm in Tm^{3+}-doped silica fiber[19]. However, before our work, there are no reports of a high-power Tm^{3+}-doped fiber laser (TDF laser, TDFL) operating on this transition.

To date, research on the 0.8 μm transition has rather focused on fluoride-based fibers[20,21]. Their lower maximum phonon energy (~500 cm^{-1}) leads to a ms-level $^3H_4$ fluorescence lifetime, so up to two orders of magnitude longer than in silica. However, the power-handling of these soft glasses limits power scaling. Currently, the highest 0.8 μm laser power from fluoride-based fibers is at the watt level[22]. Moreover, soft-glass fibers suffer from fabrication and handling (e.g., splicing) difficulties as well as hygroscopicity and/or low chemical stability. These factors highlight the preference for silica fibers, given their compatibility with existing technologies, durability and most importantly power scalability, convincingly shown in TDFs at around 2 μm as well as in Yb-doped fibers at 1–1.1 μm.

This paper reports our demonstration of 105 W of continuous-wave (CW) and 555 W of instantaneous quasi-CW (QCW) double-ended output power at 0.82 μm from an all-silica-fiber TDFL. The laser was realized using conventional down-conversion with single-step diode-laser-pumping at 0.79 μm and an in-house fabricated TDF. The laser cavity was formed by two perpendicularly cleaved fiber ends. In the QCW regime, we achieved a 0.82 μm slope efficiency of 64% versus absorbed pump power, and 54.2% versus launched power with 240 μs pulses at 40 Hz pulse repetition frequency (PRF) (duty cycle 0.96%). The 0.82 μm beam quality factor M^2 was approximately 2.2 and 2.45 in the orthogonal directions. We also demonstrate tuning over the range of 812–835 nm in a modified configuration. In

https://doi.org/10.1017/hpl.2025.10053 Published online by Cambridge University Press

the CW regime, the 0.82 μm slope efficiency was 77.5%, and the 0.82 μm optical-to-optical conversion efficiency reached 53.4%, both with respect to absorbed pump power. There was also simultaneous laser emission at approximately 1.9 μm from the $^3F_4 \rightarrow {}^3H_6$ transition. This prevented the $^3F_4$-level population from building up, which improves the pump absorption[14]. The CW and QCW (instantaneous) output power reached approximately 25 W and 54 W, respectively, at approximately 1.9 μm. Compared to our arXiv posting[23], we here present more than three times the QCW power and CW operation, as well as additional results.

2. Working principle

Our approach to single-step cladding-pumping at 0.79 μm with co-lasing at approximately 1.9 μm involves the levels $^3H_6$, $^3F_4$ and $^3H_4$. The population of other levels is small and will be disregarded. It offers several advantages. Firstly, $^3H_4$ as well as other excited levels is free from excited-state absorption (ESA) at 0.79 μm, improving efficiency and reducing the risk of photodarkening. Secondly, high-power, high-brightness 0.79 μm diode lasers are readily available, providing significant potential for power-scaling. Thirdly, pumping directly to the ULL (in-band) leads to a quantum defect that can be approximately 4% or even smaller, and thus potentially a high slope efficiency for the 0.8 μm laser. In simulations, the slope efficiency even rivaled that of YDFLs[24], which except for the co-lasing use similar configurations to in-band pumping. The approximately 1.9 μm co-lasing is indirectly beneficial for the primary $^3H_4 \rightarrow {}^3H_6$ emission at 0.8 μm. It follows on from the non-radiative decay from $^3H_4$, with power dictated by the rate of nonradiative decay from $^3H_4$. It draws on the residual $^3F_4$ energy, which is already unavailable for the 0.8 μm lasing, and beneficially makes the Tm^{3+} ions available for the pump absorption step of the 0.8 μm laser cycle. This enhances the pump absorption. Importantly, the 1.9 μm co-lasing does not depopulate $^3H_4$, so does not compete with the 0.8 μm emission and need not impair its slope efficiency or threshold.

3. Quasi-continuous-wave operation

We first consider QCW operation, for which we used pump pulses of 240 μs duration at a PRF of 40 Hz (duty cycle 0.96%).

3.1. Experimental configuration, quasi-continuous-wave operation

Figure 2 illustrates the QCW experimental setup. The TDFL comprises an 18-m-long TDF and five multimode diode lasers emitting at 0.79 μm for pumping. The TDFL emits at 0.82 μm with double-ended output. The length was chosen to yield the highest output power, although the length dependence is relatively weak around the optimum. This is expected for fiber lasers high above the threshold. The TDF is coiled on a 10 cm diameter aluminum cylinder, with no special heat dissipation measures required, thanks to the low heat generation at 0.96% duty cycle.

Figure 2 includes a cross-sectional image of the TDF. This was designed and drawn in-house from a Tm-doped silica preform designed and fabricated in-house. The TDF has a step-index core with diameter of approximately 12 μm and a numerical aperture (NA) of approximately 0.15, calculated from the preform refractive-index profile. The V-value becomes approximately 6.9 at 0.82 μm and approximately 3.0 at 1.9 μm. Surrounding the core is an octagonal pure-silica cladding ('inner cladding') with diameter of 130 μm corner-to-corner and 125 μm flat-to-flat. This is coated by a low-index acrylate for an inner-cladding NA of 0.46, nominally. For the shaping, the preform was machined in-house with a CO_2-laser prior to fiber draw.

The core propagation loss spectrum was measured with the cutback method. For this, a piece of the TDF was spliced between two pieces of SMF-28, and the transmission of light from a white light source (WLS) was measured

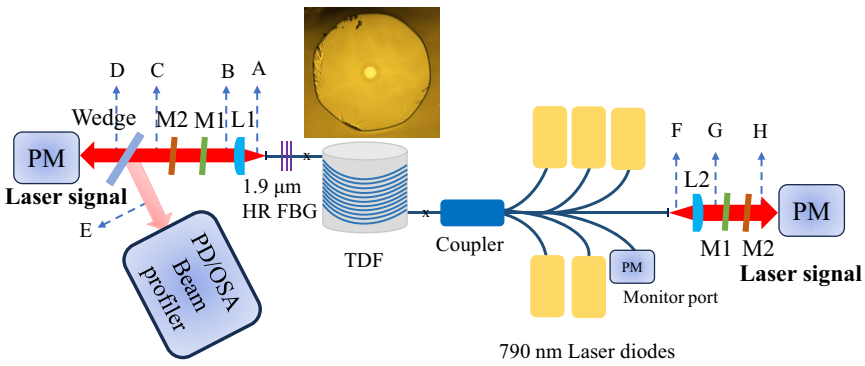

Figure 2. Experimental setup of the TDFL. TDF, thulium-doped fiber; FBG, fiber Bragg grating; PM, power meter; PD, photodetector; OSA, optical spectrum analyzer; L1, L2, antireflection-coated collimating lens; M1, short-pass filter, with cut-off wavelength 1600 nm; M2, long-pass filter, with cut-on wavelength 800 nm. A, B, C, D, E, F, G and H, reference positions for measurements. Inset: microscope image of the TDF (130 μm diameter corner-to-corner).

https://doi.org/10.1017/hpl.2025.10053 Published online by Cambridge University Press

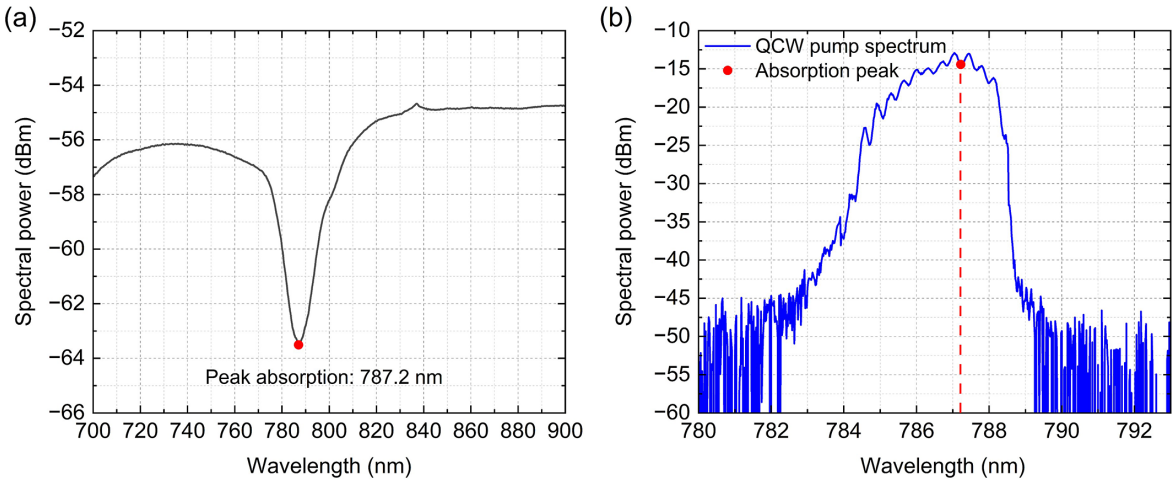

Figure 3. (a) Measured white light ('cold') cladding transmission spectrum in 15 m of TDF (RBW: 0.1 nm). (b) Combined QCW spectrum of all five 0.79 μm diode lasers at full pump power.

with an optical spectrum analyzer (OSA) for two different TDF lengths. The core propagation loss at 0.82 μm is approximately 0.25 dB/m, comprising both ground state absorption (GSA) of Tm^{3+} ions and background loss. This is the 'cold' loss, with all Tm^{3+} ions in the ground state. At 1.32 μm, the background loss is approximately 0.15 dB/m. This wavelength avoids both Tm^{3+} GSA and OH^- absorption. The OH^- core absorption at 1380 nm was measured to approximately 0.35 dB/m, from which we estimate the core's OH^- concentration to around 7 ppm (parts per million).

To assess the pump absorption, the 'cold' absorption for light propagating in the inner cladding was measured with a WLS in 15 m of TDF laid out in a loose 10-cm-diameter coil. It reaches approximately 9 dB at the absorption peak of 787.2 nm (Figure 3(a)). Although the cladding edges appear somewhat rounded in the inset of Figure 2, bending the TDF to mix the pump modes did not enhance the absorption, as it does with circularly symmetric fibers[25]. This suggests that the cladding shaping successfully negated detrimental mode-selective pump depletion.

The TDF was cladding-pumped by five 0.79 μm fiber-coupled diode lasers (BWT diodes, K793DL9RN) launched via a (6 + 1) × 1 pump and signal combiner with six pump ports (Lasfiberio, pump fiber, Coherent MM-S105/125-22A; signal and common-port fiber, Coherent SM-GDF-10/130-15M, low index acrylate coating). This was spliced to the TDF. One pump port was left unconnected and instead used to indirectly monitor the backward-propagating 0.82 μm power entering the diode lasers spliced to the other pump ports. This was a precaution, as the diode lasers are only protected internally over the 1900–2100 nm range. Under QCW pumping, the diode lasers were driven in series by diode laser drivers (LDD-1046, 120A/120V, Meerstetter), capable of fast-pulse operation (on and off switching times <10 μs). The drivers were controlled by 250 μs rectangular pulses at a PRF of 40 Hz from a waveform generator (Tektronix AFG31152, 150 MHz bandwidth, 2 GSa/s sampling rate) via their current control ports. This resulted in rectangular pump pulses of 240 μs duration (duty cycle 0.96%). The pump diodes are rated at 130 W of CW power in a 105 μm core fiber with an NA of 0.22. In QCW operation with 240 μs pulses, they can be driven to produce around approximately 230 W of instantaneous pump power for a total of approximately 1.15 kW. The pump transmission of the combiner was measured to approximately 94%. The total maximum instantaneous pump power exiting from the combiner into free space was measured to 1.08 kW. Compensating for the Fresnel loss and neglecting splice loss, 1.12 kW of maximum instantaneous pump power was launched into the TDF, limited by available pump power. The emission spectrum of the pump lasers at full power is well matched to the TDF absorption peak (Figures 3(a) and 3(b)). We measured the pump leakage to around –7.87 dB (loss ~0.437 dB/m) at full power.

The 0.82 μm laser cavity was formed by perpendicular fiber cleaves in both ends of the fiber assembly with Fresnel-reflection feedback of 3.5% at 0.82 μm. The laser output power is therefore double-ended. A high-reflection fiber Bragg grating (FBG) to make the output single-ended was not available. Also for the 1.9 μm laser cavity, the Fresnel reflection (3.2%) from the perpendicularly cleaved fiber end provided the feedback in the pump launch end. In addition, a high-reflection FBG (TeraXion, fiber, Coherent SM-GDF-10/130-15M, low index acrylate coating) was spliced to the far end of the TDF to close the cavity. Compared to 3.2% Fresnel reflection, this reduces the required $^3F_4$–$^3H_6$ inversion and, advantageously, the number of ions in $^3F_4$.

At both ends of the fiber cavity, antireflection (AR) coated Infrasil aspheric lenses (L1 and L2, NA ~ 0.35, AR range 0.8–2 μm, Laser 2000) collimated the output beams. Although the NA of the lens is smaller than that of the inner cladding, it was able to collect all the light exiting the

https://doi.org/10.1017/hpl.2025.10053 Published online by Cambridge University Press

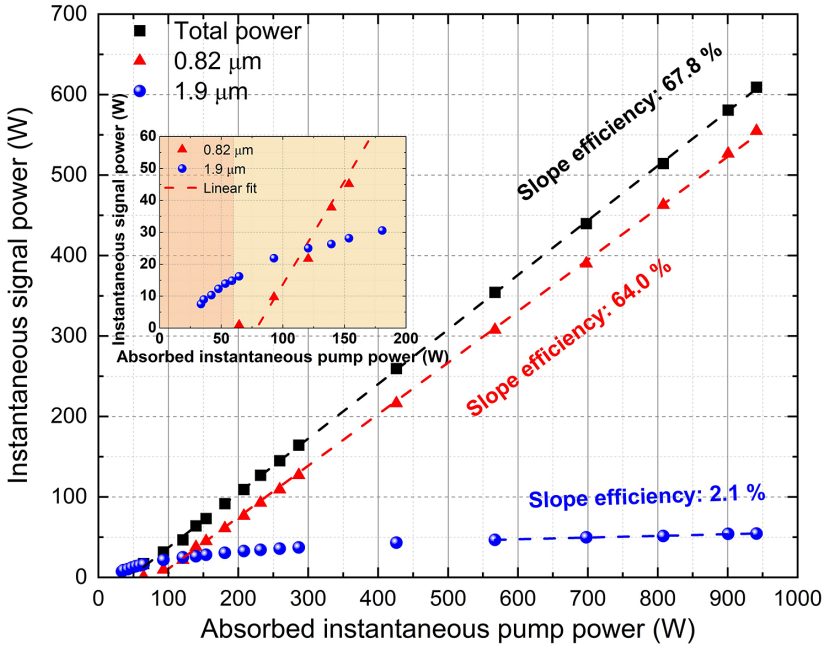

Figure 4. QCW instantaneous output power combined from both ends of the TDFL versus absorbed instantaneous pump power. Blue dots, power at 1.9 nm; red triangles, power at 0.82 μm; black squares, total output power. Inset: enlarged view of the behavior near the threshold.

fiber ends. To separate out the 0.82 μm beams, short-pass filters M1 (1600SP, Edmund Optics) and long-pass filters M2 (FELH800, Thorlabs) removed the residual pump and the 1.9 μm co-lasing power. The combination induced a loss of approximately 0.70 dB at 0.82 μm. In addition, an uncoated wedge was used intermittently to sample the laser output for characterizations including the temporal trace, spectrum and beam quality.

We determined instantaneous QCW powers by measuring average powers with thermal power meters and dividing by the 0.96% duty cycle. Quoted powers and efficiencies for 0.82 μm are based on data measured at positions C and H in Figure 2, which are then recalculated to positions A and F. The 1.9 μm power was measured in a similar manner by replacing M1 with a long-pass filter (FELH1000, Thorlabs, not shown in Figure 2) to directly measure the power afterwards. The value was then recalculated to position F. Thus, the losses in the lenses and filters are compensated for in the presented results by 0.70 dB at 0.82 μm and by 0.46 dB at 1.9 μm. We also measured the leaked pump and compensated for its outcoupling losses in the data we report.

Diagnostic equipment of note were a Thorlabs DET10A/M biased silicon photodetector (PD) with 350 MHz bandwidth, a Thorlabs DET10D2 biased InGaAs PD with 14 MHz bandwidth, a Keysight InfiniiVision MSOX3104G oscilloscope with 1 GHz bandwidth, an Ophir FL250A-BB-50-PPS beam tracking power and energy sensor, an Ophir 150 W power meter with a thermopile detector and a Thorlabs dual-scanning-slit beam profiler (BP209VIS/M) mounted on an M^2 measurement system with a motorized translation stage (M2MS). For optical spectra, we used Ando AQ6317B and Yokogawa AQ6376 OSAs.

3.2. Quasi-continuous-wave laser results

Figure 4 shows the instantaneous laser output power at 0.82 and 1.9 μm as a function of the absorbed instantaneous pump powers in the QCW regime. Here and throughout, we take the absorbed pump power to be the difference between launched and leaked pump powers (leakage –7.87 dB, i.e., 16.3%, at full power, corresponding to around 183 W). The 1.9 μm laser threshold is lower than the 0.82 μm threshold. This is understandable, since the lifetime of $^3F_4$ is much longer than that of $^3H_4$. We could not investigate the characteristics below an instantaneous pump power of around 33 W (current of 3.68 A) because the diode drivers were unable to reliably generate lower currents.

The instantaneous absorbed pump threshold power for 0.82 μm laser emission was approximately 60 W (~75 W launched). The short lifetime of the ULL $^3H_4$ and the high cavity loss contribute to the high threshold, which we believe is among the highest reported for a cladding-pumped fiber laser. Although a high threshold is undesirable, it is still only a small fraction of the available QCW pump power. This underlines the opportunity offered by the high power and brightness of state-of-the-art diode lasers. Thus, at the maximum launched instantaneous pump power of 1.12 kW, approximately 555 W of instantaneous 0.82 μm output power was obtained, combined from both output ends. The forward and backward powers were nearly the same, which indicates that both ends of the cavity were equivalent and thus that the splices and cleaved fiber facets were good. The 0.82 μm slope efficiency with respect to the absorbed pump power reaches 64%. The output power increases linearly with an increase in the pump power, without any power

https://doi.org/10.1017/hpl.2025.10053 Published online by Cambridge University Press

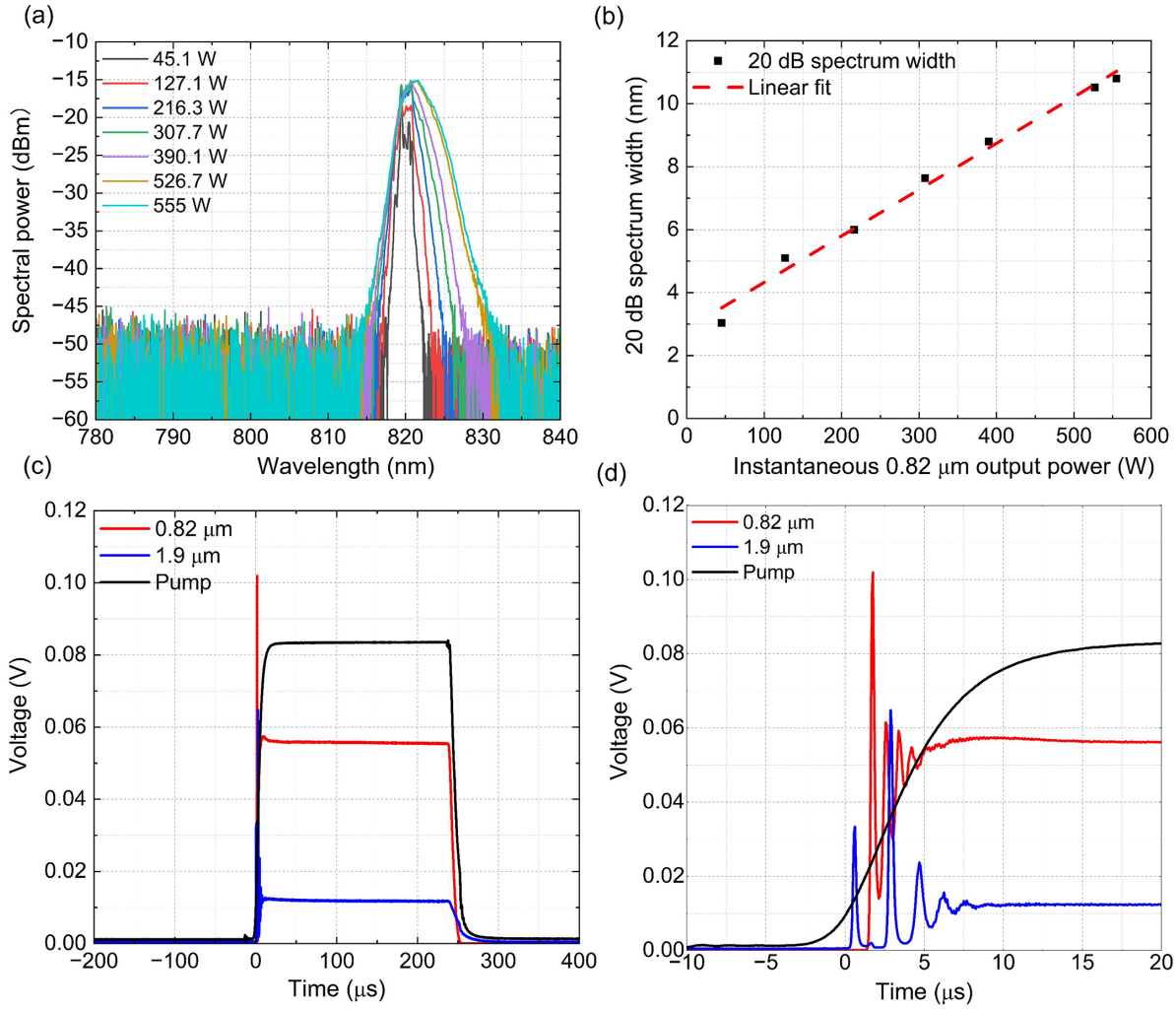

Figure 5. QCW measurements. (a) Optical spectrum at different 0.82 μm output power (RBW: 0.2 nm). (b) 20 dB spectral width versus 0.82 μm output power. (c) Time traces of the laser output at 0.82 and 1.9 μm of the 0.79 μm pump at full power. (d) Enlarged view showing the relaxation oscillation process.

roll off. It is noteworthy that at full power, approximately 10 W of instantaneous power, predominantly at 0.82 μm, was measured at the combiner's pump port used for monitoring. This stems from the portion of the generated signal light that leaks into the cladding, for example at splices or as bendloss higher order modes. Even if it does not contribute to the useful output, it does add to the intrinsic conversion efficiency of the TDF. Assuming that all pump ports contain a similar backward-propagating 0.82 μm power, this adds up to approximately 60 W, which is not included in the output powers or slope efficiencies we report.

Above its threshold, the 1.9-μm output power first increases with a slope of approximately 32% with respect to absorbed pump power. The wavelength was centered at around 1901 nm as determined by the FBG. Then, above the 0.82 μm laser threshold, the 1.9 μm slope drops to only 2.1%. Indeed, in the ideal case of a 'homogeneous' gain medium with all Tm^{3+} ions being spectroscopically equal and negligible temperature effects, the 0.82 and 1.9 μm laser fields clamp the populations of the three populated levels. This in turn clamps the nonradiative decay from $^3H_4$ to $^3F_4$ and thus the stimulated emission from $^3F_4$ to $^3H_6$ in the ideal case. Although 2.1% is small, if the differential loss of this channel were instead funneled into 0.82 μm emission (as it might be, with homogeneous gain characteristics), it could add approximately $(1.9 / 0.82) \times 2.1\% = 4.86\%$ to the 0.82 μm slope. The instantaneous power at approximately 1.9 μm reached approximately 54.4 W at full power, so approximately 10% of the 0.82 μm power and 18.5% of the total number of photons in the laser output. No degradation in output power was observed during our measurements.

The 0.82 μm output spectrum at different pump power was measured with an OSA (Ando, AQ6317B), triggered synchronously with the pulses; see Figure 5(a). The output spectrum was centered at 821.6 nm at full power. The spectral width increased linearly with 0.82 μm output power from 3 to 11 nm, as shown in Figure 5(b). A large linewidth is expected since the cavity has no spectrally narrow selection

https://doi.org/10.1017/hpl.2025.10053 Published online by Cambridge University Press

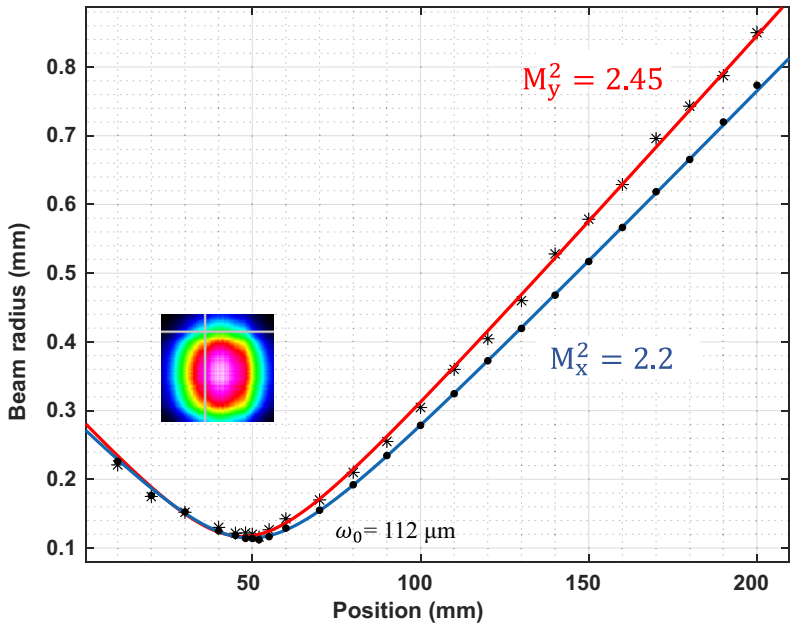

Figure 6. Measured 0.82 μm beam radius in the orthogonal directions at different longitudinal positions at approximately 250 W of instantaneous power. Inset: synthetic two-dimensional (2D) 0.82 μm beam profile as reconstructed by the scanning-slit beam profiler.

for the $^3H_4 \rightarrow {}^3H_6$ emission. The further broadening at higher power may be caused by increased spectral competition as well as by self-phase modulation (SPM), as the nonlinear phase shift is not negligible, according to calculations. Stimulated Raman scattering would occur at approximately 0.85 μm. This was not observed over the effective noise level of approximately 4 mW in the 0.2 nm resolution bandwidth (RBW; determined from Figure 5(a)).

Figure 5(c) shows temporal traces of the pump and the 0.82 and 1.9 μm output. The overall temporal characteristics of the TDFL largely follow those of the diode drivers. The difference in duration and thus duty cycle between the three traces is negligible. Figure 5(d) zooms in on the switch-on characteristics. The pump switches on within 10 μs (10%–90%). Relaxation oscillation at 1.9 and 0.82 μm occurs, respectively approximately 3 and 5 μs after the pump power starts to rise. These die out before the pump power is fully on. Efficient operation remained possible with pulses down to approximately 100 μs duration.

The beam quality factor (M^2) of the 0.82 μm output was measured at a launched pump power of 640 W with the scanning-slit beam profiler in pulse measurement mode. This was measured in the pump launch end, at position E in Figure 2. The results are shown in Figure 6. The M^2-factor was determined to be 2.2 (beam parameter product (BPP), 0.57 mm mrad) and 2.45 (0.64 mm mrad) in the orthogonal directions, based on a hyperbolic fit to the beam width as measured at the $1/e^2$ intensity level. This is consistent with the passive output fiber's V-number of 5.75 at 0.82 μm.

In addition, we investigated the tuning characteristics of the TDFL in the QCW regime. For this, the far output end of a 19-m-long piece of the TDF (near position A in Figure 2) was angle-cleaved to suppress feedback. Instead, a Littrow-configured diffraction grating located at position B with approximately 70% reflectivity at 0.82 μm provided wavelength-selective feedback, tunable by adjusting the angle of incidence. In a non-optimized experiment, the laser was then generated between 129 and 152 W of instantaneous single-ended output power with continuous tuning from 812 to 835 nm for a launched instantaneous pump power of 427 W; see Figure 7. The slope efficiency was approximately 50.9%. The 23 nm tuning range corresponds to 10.2 THz, which suggests that Gaussian-shape pulses as short as 40 fs can be amplified. Wider and shifted tuning ranges are expected with tailored TDF parameters and configurations[26].

4. Continuous-wave operation

4.1. Experimental configuration, continuous-wave operation

Figure 8 illustrates the CW experimental setup. The configuration is largely the same as the QCW setup, but with the following differences. The 0.79 μm diode lasers were driven in series by TDK Lambda Genesys 100-15 power supplies.

Two perpendicular fiber facets were used to form the 1.9 μm cavity as the FBG used QCW was damaged under high-power CW operation. We believe this was a result of excessive leaked pump power. Thus, we replaced the FBG with a short piece of passive fiber (SM-GDF-10/130-15M, Coherent) spliced to the TDF and with a perpendicularly cleaved output end. As a result, the 0.8 and 1.9 μm bands shared the same cavity.

https://doi.org/10.1017/hpl.2025.10053 Published online by Cambridge University Press

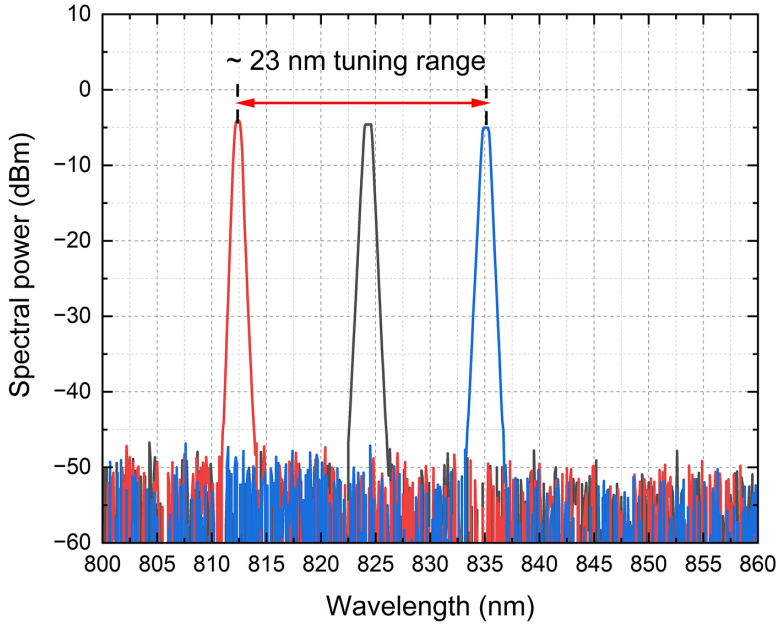

Figure 7. Measured output spectra of the wavelength-tunable QCW TDFL at over 100 W of instantaneous output power in the 0.8 μm band (RBW: 0.5 nm).

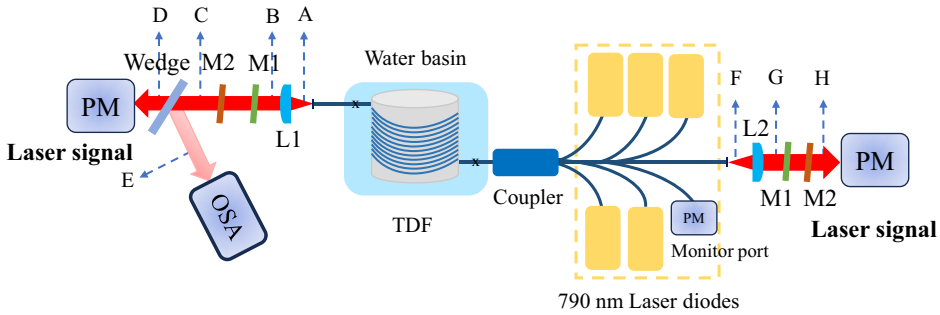

Figure 8. Schematic of a CW TDFL with two perpendicularly cleaved ends.

For thermal management, the 0.79 μm diode lasers and pump combiner were mounted on a water-cooled aluminum heatsink. We reiterate that for CW the diode lasers are rated at approximately 130 W, which is significantly lower than the approximately 230 W of instantaneous power we used for the QCW. However, damage at the splice between the pump combiner and the TDF limited the CW pump launch into the TDF to approximately 291 W of total power (neglecting the splice loss). The power of individual diode lasers was then approximately 62 W on average before the combiner.

The active fiber, reduced to approximately 17 m in length due to loss from damage and splice repairs, was wound onto a 13-cm-diameter metal cylinder and fully submerged in water. Also, the splices to the TDF were submerged in order to prevent damage from occurring at low power. The water temperature was between 15°C and 20°C. These were our primary heatsinking measures. We did not use any heat-conductive foil or paste or machined grooves to improve thermal contact between the fiber and the cylinder.

Figure 9 shows individual diode laser spectra at approximately 130 W of individual power, together with a pump absorption spectrum measured in the same way as in Figure 3. The spread of the central wavelengths is approximately 2 nm and the linewidth of individual diode lasers is also approximately 2 nm. Overall, the spectral match is good, with the diode lasers being marginally too long in wavelength relative to the absorption peak. However, this is at 130 W, whereas the highest used individual diode laser power was approximately 62 W. This reduction in power shifts the spectrum to approximately 3 nm shorter wavelengths. The reduction in absorption due to the spectral mismatch is less than 1 dB from the peak value.

4.2. Continuous-wave laser results

Figure 10(a) shows how the measured laser output power depends on the pump power. The pump threshold power for 0.82 μm laser emission with our two 3.5% reflecting facets was approximately 50 W (absorbed) and approximately 67.4 W (launched). The threshold for the 1.9 μm laser emission (now double-ended) is approximately 10 W.

https://doi.org/10.1017/hpl.2025.10053 Published online by Cambridge University Press

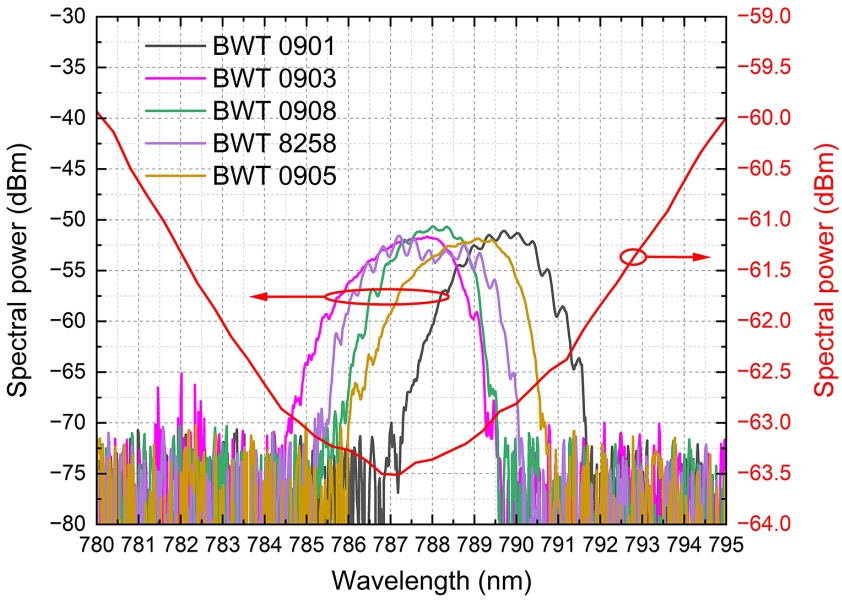

Figure 9. Left axis: individual diode laser spectra. Right axis: cladding absorption spectrum of the TDF (RBW: 0.1 nm).

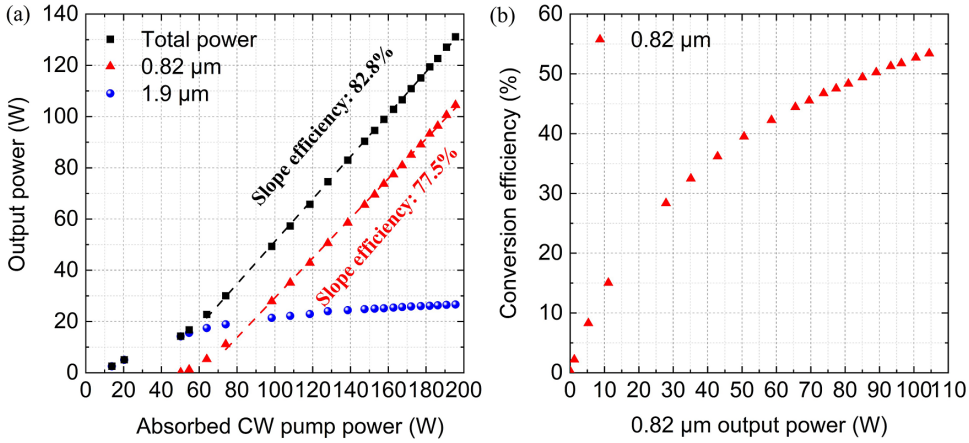

Figure 10. (a) CW output power combined from both ends of the TDFL versus absorbed pump power. Blue dots, power at 1.9 nm; red triangles, power at 0.82 μm; black squares, total output power. (b) Conversion efficiency of 0.82 μm with respect to absorbed pump power versus 0.82 μm laser output power.

The 0.82 μm output power reached 105 W at the maximum absorbed pump power of 196 W (291 W launched). This was limited by failure at the splice between the pump combiner and the TDF. The slope efficiency of the 0.82 μm emission with respect to absorbed pump power was 77.5%, without any sign of roll off. This is a notable improvement over the 64% obtained QCW. If we include the 1.9 μm emission to calculate an overall slope efficiency for the laser output, then this becomes around 83%. This sets a limit on the differential heat generation and may be a record slope efficiency for any TDFL cladding-pumped by diode lasers, or even any diode-laser-pumped Tm^{3+}-doped laser, at output power above 100 W.

Figure 10(b) presents the optical-to-optical conversion efficiency from absorbed pump to 0.82 μm output power as a function of the output power. At output powers below, say, 20 W, the conversion efficiency suffers from the high laser threshold. However, the conversion efficiency improves to over 50% at an output power of 100 W. FBGs at 0.82 μm may reduce the threshold and thus improve the efficiency at lower power.

The 0.82 μm output spectrum at full power is illustrated in Figure 11, showing a background that is more than 50 dB below the spectral peak as measured with 2 nm RBW. Any stimulated Raman scattering would peak at approximately 0.85 μm or shorter but was not observed, nor was any spectral broadening caused by the Kerr nonlinearity.

The 196 W of absorbed pump power at the full launched pump power of 291 W implies a pump leakage of 95 W, that is, –4.86 dB (32.7%), which is high. Figure 12 illustrates how

https://doi.org/10.1017/hpl.2025.10053 Published online by Cambridge University Press

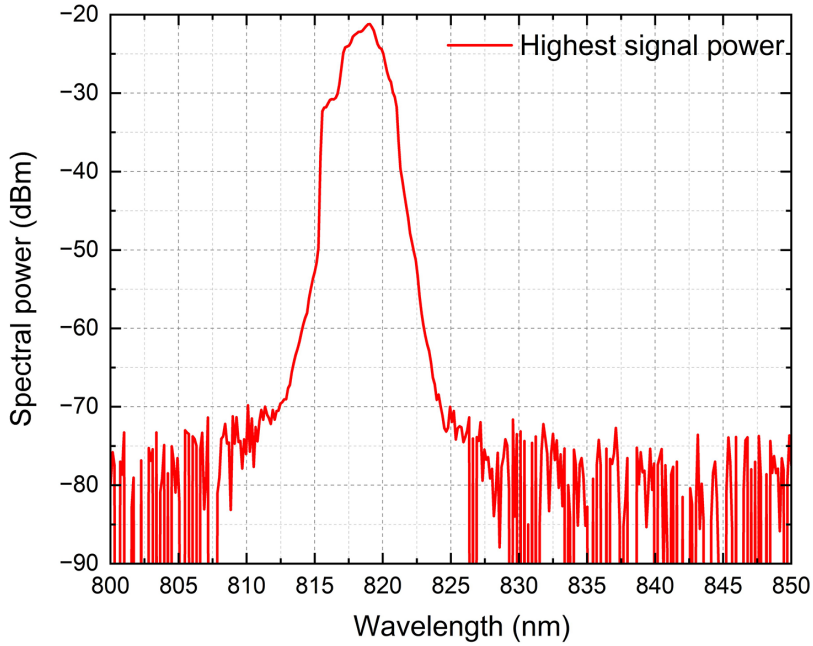

Figure 11. CW output spectrum at full power (RBW: 2 nm).

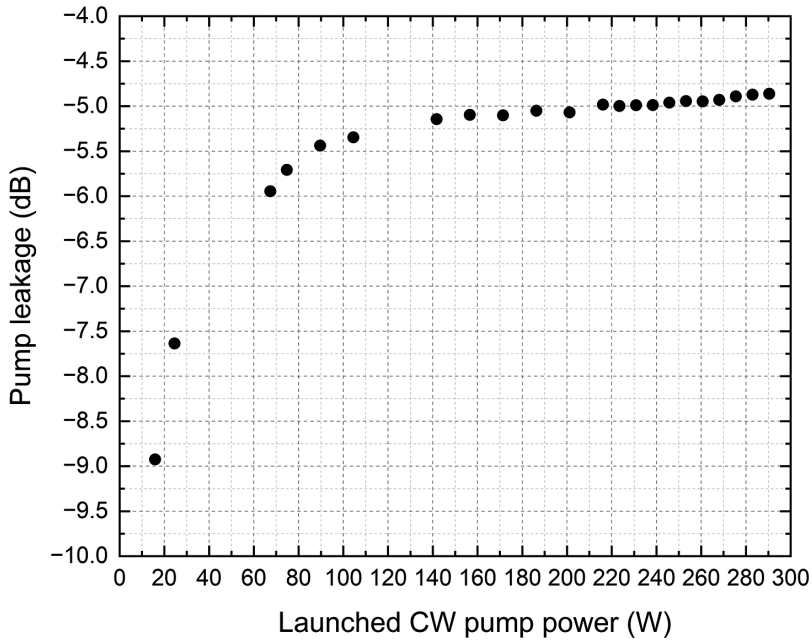

Figure 12. CW pump leakage versus launched pump power.

the pump leakage varies with launched pump power. At low pump levels, the leakage reaches 9 dB, in good agreement with the WLS transmission spectrum in Figure 3. As the pump power increases, the leakage rises rapidly, reaching –6 dB at the 0.82 μm threshold of 67.4 W. We attribute this primarily to the reduced population of Tm^{3+} ions in the ground state as the threshold is approached. Beyond the threshold, the leakage increases only gradually, by about 1 dB at full power. This slow increase may result from thermal effects in the diode lasers and/or the TDF, which would be consistent with the lower leakage observed in the QCW case. Note that the TDF length was optimized for QCW operation. A longer TDF and improved heatsinking may reduce the pump leakage and allow for higher CW output power.

We operated the system at maximum power for no more than approximately 10 min. Except for catastrophic failures, no noticeable degradation in laser performance (e.g., from photodarkening) was observed. Additional characterization is needed to establish long-term reliability.

https://doi.org/10.1017/hpl.2025.10053 Published online by Cambridge University Press

5. Discussion

MPR from $^3H_4$ feeds the $^3F_4$ population, which detrimentally reduces the number of Tm^{3+} ions available for the primary $^3H_6$–$^3H_4$ transition. To estimate this, we first evaluated the fractional populations of the levels $^3H_6$ (n_1), $^3F_4$ (n_2) and $^3H_4$ (n_3) as averaged over the TDF from the spectroscopic cross-sections and the laser gain thresholds. For this, we used absorption and emission cross-sections σ_a and σ_e determined on other TDFs. At 0.82 μm, $\sigma_a = 0.244 \times 10^{-25}$ m^2 and $\sigma_e = 2.40 \times 10^{-25}$ m^2. At 1.9 μm, $\sigma_a = 0.253 \times 10^{-25}$ m^2 and $\sigma_e = 3.83 \times 10^{-25}$ m^2. In the QCW configuration with an 18-m-long TDF and a cavity roundtrip loss estimated to 30 dB at 0.82 μm and 16 dB at 1.9 μm, we get $n_1 = 0.811$, $n_2 = 0.067$ and $n_3 = 0.123$. The excited ions reduce the 'hot' pump absorption by a fraction $1 - n_1 + n_3 \cdot (\sigma_e / \sigma_a) = n_2 + n_3 (1 + \sigma_e / \sigma_a) = 0.2986$, approximately, where the cross-section values are those of the pump with σ_e / σ_a taken to be 0.8918. Given a 'cold' pump absorption of approximately 9 dB, this suggests a 'hot' pump absorption of approximately 6.3 dB. The difference in the –7.87 dB measured pump leakage may partly be caused by background propagation and splice loss. If $^3F_4$ is empty ($n_2 = 0$) then the 'hot' pump absorption becomes around 0.50 dB higher. This suggests that although the finite population of $^3F_4$ reduces the pump absorption, the effect is small and has little impact on the 0.82 μm characteristics in this QCW case.

It is also possible to assess an operating $^3H_4 \rightarrow {}^3F_4$ relaxation rate (dominated by MPR) from the $^3H_4$ population ($n_3 = 0.123$ QCW) and the 1.9 μm power. For example, 20 W of 1.9 μm output power (near the 0.82 μm threshold and generated at a launched pump power of 100 W) corresponds to 1.91×10^{20} photons per second. Furthermore, with $n_3 = 0.123$, there are approximately 4.99×10^{15} Tm^{3+} ions in $^3H_4$. From this, the operating $^3H_4 \rightarrow {}^3F_4$ relaxation rate becomes $(26.1\ \mu s)^{-1}$. At 50 W of 1.9 μm power (launched pump power ~844 W), the operating relaxation rate becomes $(10.4\ \mu s)^{-1}$. This assumes that the $^3H_4$ population is clamped to $n_3 = 0.123$, which need not be in the presence of inhomogeneities or temperature effects, although the latter are small in the QCW regime.

The $(26.1\ \mu s)^{-1}$ operating relaxation rate is consistent with the initial decay of the 0.8 μm fluorescence following excitation of the $^3H_4$ level by approximately 100 W, and 0.79 μm pump pulses are launched into the inner cladding. We measured the fluorescence in the backward direction from a piece of the TDF short enough to avoid reabsorption and stimulated-emission effects. The decay was non-exponential and depended on the pump pulse duration. A pump duration of 20 μs resulted in an initial decay rate of $(20.0\ \mu s)^{-1}$ (1.31 μs after the pump was switched off), a fall time to 1/*e* of 21.5 μs and a decay rate of $(57.2\ \mu s)^{-1}$ in the long tail. A pump duration of 5 μs resulted in an initial decay rate of $(18.1\ \mu s)^{-1}$ (1.16 μs after the pump was switched off), a fall time to 1/*e* of 19.5 μs and a decay rate of $(52.4\ \mu s)^{-1}$ in the long tail.

The higher calculated MPR rate of $(10.4\ \mu s)^{-1}$ with 844 W of instantaneous launched pump power may be the result of an increased participation of short-lived ions in the laser cycle at higher power. We also note that our results suggest that the slow decay in the long tail is less relevant. See Refs. [15, 16] and references therein for further discussions of the $^3H_4$ lifetime in silica fiber.

The short $^3H_4$ lifetime is a disadvantage. Nevertheless, with the QCW, the exceptional launched instantaneous pump power of 1.12 kW (~88.4 mW/μm^2 intensity) allows us to operate well above the approximately 75 W threshold (~5.1 mW/μm^2 launched intensity) of our configuration, even with single-ended pumping and one pump port unused. We also estimate the pump needed locally for 0 dB/m Tm-ion gain at 0.82 μm to 2.83 mW/μm^2 and thus 42 W in total if spread out evenly across the inner cladding. Although the uncertainty in this estimate is large, this would be the minimum power for local gain and thus the minimum leaked power at full power, disregarding background loss. Again, although this is a high value for a fiber laser, it is still much smaller than the launched pump power. However, with the CW, the threshold as well as the minimum power for local gain constitutes a significant fraction of the failure-limited pump power. Higher power may be possible with improved thermal resilience (e.g., better coating, stripping or heatsinking) or reduced thermal load per unit length (e.g., lower Tm^{3+} concentration). The diode lasers themselves would allow for over 800 W of single-ended pump power if we use all six pump ports, and approximately 1600 W with double-ended pumping. However, such high pump power (which would make the threshold negligible also the CW) has not been demonstrated with an approximately 125-μm-diameter pump waveguide and may rather require a diameter of 250 or 400 μm. The threshold will be higher, but not overly so in an optimized laser. Note that 400 μm Yb-doped fibers allow for several kW of pump power in commercial high-power lasers.

Even when the pump power is not limited, the complex spectroscopy of Tm^{3+} contains many potential channels for loss (including nonlinear loss), which may also hamper power-scaling. Nevertheless, the lack of roll off QCWs as well as CWs does indicate higher power is possible. The potential seems significant, and if the low 4% quantum defect is fully reflected by a low thermal load, then multi-kW CW operation may well be possible.

Operation at lower power (say, 10 W) is also of interest, but in this regime, the high threshold hampers the efficiency; see Figure 10(b). A smaller pump waveguide (e.g., 80 μm), a smaller core and longer $^3H_4$ lifetime can help to reduce the threshold. It is also possible to reduce the outcoupling and thus the cavity loss, although this typically also reduces the

https://doi.org/10.1017/hpl.2025.10053 Published online by Cambridge University Press

slope efficiency. We also note that QCW operation enables high efficiency at low average power.

6. Conclusion

We have demonstrated approximately 105 W of output power CW and approximately 555 W of instantaneous output power QCW at 0.82 μm from an all-silica-fiber thulium-doped fiber laser. The TDF was designed and fabricated in-house and was cladding-pumped by pigtailed diode lasers at 0.79 μm. Population trapping in $^3F_4$ was counteracted by co-lasing at 1.9 μm. Under QCW pumping with pulse duration of approximately 240 μs and a repetition rate of 40 Hz, the 0.82 μm slope efficiency reached 64% versus absorbed pump power, and 54.2% versus launched power. The measured beam quality M^2 at approximately 250 W instantaneous output power was 2.2 (BPP: 0.57 mm mrad) and 2.45 (BPP: 0.64 mm mrad) in the orthogonal directions. Moreover, a modified configuration with a diffraction grating was continuously tunable from 812 to 835 nm.

In CW operation, the 0.82 μm slope efficiency was 77.5% with respect to absorbed pump power. The achieved output power of 105 W at 0.82 μm was limited by failure at a splice. The high MPR rate of the ULL $^3H_4$ leads to a high threshold of approximately 50 W of absorbed pump power. However, at high power, the impact of this on the conversion efficiency is small, thanks to the use of high-power, high-brightness pump diode lasers. Thus, the optical-to-optical conversion efficiency reached 53.4% with respect to absorbed pump power. The single-pass 0.82 μm gain was as high as 15 dB in our configuration, thus pointing to the possibility of a 0.82 μm fiber amplifier offering simultaneous high gain, high power and high efficiency.

The low quantum defect (e.g., 4%) is a primary attraction of a 0.82 μm TDFL. If this is fully reflected by a low thermal load, then CW multi-kW operation may well be possible. To the best of our knowledge, this is the first experimental demonstration of a high-power silica-based fiber laser source operating in the 800 nm range. We believe these results enable a broad range of applications through a robust and reliable diode-pumped all-fiber laser source.

Acknowledgements

This work was funded by the Air Force Office of Scientific Research (FA9550-17-1-0007), EPSRC EP/T012595/1 (LITECS). Changshun Hou thanks the China Scholarship Council for financial support (Grant No. 202206160003). Jiaying Wu processed the fluorescence decay data.

References

1. S. Li, X. Yue, Q. Li, H. Peng, B. Dong, T. Liu, H. Yang, J. Fan, S. Shu, F. Qiu, and Q. Jiang, J. Mater. Res. Technol. **27**, 944 (2023).
2. V. Ferreira, P. Egizabal, V. Popov, M. G. de Cortázar, A. Irazustabarrena, A. López-Sabirón, and G. Ferreira, Diamond Relat. Mater. **92**, 174 (2019).
3. A. Demirkesen and M. Ucar, in *International Marmara Science Congress* (2020), p. 161.
4. M. Dündar and G. Güngör, *Report Assan Aluminum* (İstanbul, 2008).
5. M. Fabian, E. Lewis, T. Newe, and S. Lochmann, Meas. Sci. Technol. **21**, 094034 (2010).
6. D. Bergstrom, "The absorption of laser light by rough metal surfaces", PhD. Thesis (Luleå University of Technology, 2008).
7. Ł. Łach, Crystals **14**, 726 (2024).
8. Y. Takeuchi, M. Uehara, K. Kohno, M. Musha, K. Nakagawa, and K. Ueda, in *CLEO Europe* (2013), paper CJ_8_6.
9. V. Ligeret, F. Vermersch, S. Bansropun, M. Lecomte, M. Calligaro, O. Parillaud, and M. Krakowski, in *CLEO* (2006), paper JWB5.
10. L. Antoni-Micollier, M. Viteau, B. Battelier, B. Cadier, D. Comparat, B. Desruelle, G. Guiraud, E. Pinsard, M. Reveillard, S. Rota-Rodrigo, G. Stern, N. Traynor, and G. Santarelli, Opt. Lett. **43**, 3937 (2018).
11. R. Florentin, A. Viry, K. Le Corre, T. Robin, T. Georges, G. Santarelli, H. Gilles, S. Girard, and M. Laroche, Opt. Lett. **50**, 1476 (2025).
12. Y. Chen, Z. Lin, H. Sun, Y. Wang, H. Dong, M. Wang, L. Zhang, G. Dong, X. Liu, F. Yu, S. Wang, C. Yu, and L. Hu, Optica **10**, 905 (2023).
13. I. V. Obronov, A. S. Demkin, and D. V. Myasnikov, Quantum Electron. **48**, 212 (2018).
14. D. J. B. Brinck, "An investigation of the spectroscopy and laser performance of thulium in a variety optical fiber hosts", PhD. Thesis (University of Southampton, Faculty of Science, 1996).
15. P. Vařák, M. Leich, M. Kamrádek, J. Aubrecht, O. Podrazký, I. Bartoň, B. Švejkarová, A. Michalcová, K. Wondraczek, M. Jäger, I. Kašík, P. Peterka, and P. Honzátko, J. Luminescence **275**, 120835 (2024).
16. S. Unger, M. Leich, A. Schwuchow, M. Lorenz, R. Müller, A. Pratiwi, J. Kobelke, A. Lorenz, J. Dellith, C. Kränkel, and M. Jäger, Opt. Mater. Express **15**, 446 (2025).
17. P. Peterka, I. Kasik, A. Dhar, B. Dussardier, and W. Blanc, Opt. Express **19**, 2773 (2011).
18. P. R. Watekar, S. Ju, and W.-T. Han, IEEE Photon. Technol. Lett. **18**, 1651 (2006).
19. C. Hou, D. Pal, C. C. Baker, T. Zhou, D. Rhonehouse, J. Sanghera, and J. Nilsson, EPJ Web Conf. **307**, 02045 (2024).
20. E. Kajikawa, T. Ishii, K. Ogawa, and M. Musha, Appl. Opt. **60**, 6776 (2021).
21. E. Kajikawa, T. Ishii, T. Kubo, Y. Takeuchi, K. Ogawa, and M. Musha, Opt. Lett. **44**, 2875 (2019).
22. J. Wang, Z. Jia, Y. Ren, C. Zhang, Y. Ohishi, W. Qin, and G. Qin, Opt. Lett. **48**, 6476 (2023).
23. C. Hou, Z. Zhai, N. Choudhury, T. Harris, J. K. Sahu, and J. Nilsson, arXiv:2412.01793 (2024).
24. E. Mejia-Beltran, L. A. Zenteno, P. Gavrilovic, and A. K. Goyal, Opt. Eng. **37**, 2699 (1998).
25. P. Koška, P. Peterka, J. Aubrecht, O. Podrazký, F. Todorov, M. Becker, Y. Baravets, P. Honzátko, and I. Kašík, Opt. Express **24**, 102 (2016).
26. J. Nilsson, W. A. Clarkson, R. Selvas, J. K. Sahu, P. W. Turner, S. U. Alam, and A. B. Grudinin, Opt. Fiber Technol. **10**, 5 (2004).

https://doi.org/10.1017/hpl.2025.10053 Published online by Cambridge University Press